

# Development of Micromegas-based Active-Target Time Projection Chamber for Nuclear Astrophysics Studies

Pralay Kumar Das<sup>1\*</sup>, Nayana Majumdar<sup>1</sup> and  
Supratik Mukhopadhyay<sup>2</sup>

<sup>1\*</sup>Applied Nuclear Physics Division, Saha Institute of Nuclear Physics,  
A CI of Homi Bhabha National Institute, 1/AF Block, Bidhannagar,  
Kolkata, 700064, West Bengal, India.

<sup>2</sup>Research Wing, Naihati Prolife, Naihati, West Bengal, India.

\*Corresponding author(s). E-mail(s): [pralay.das@saha.ac.in](mailto:pralay.das@saha.ac.in);  
Contributing authors: [nayana.majumdar@saha.ac.in](mailto:nayana.majumdar@saha.ac.in);  
[supratikmukhopadhyay.sinp@gmail.com](mailto:supratikmukhopadhyay.sinp@gmail.com);

## Abstract

A Micromegas-based active-target detector named SAT-TPC (Saha Active Target TPC) has been designed and fabricated at the Saha Institute of Nuclear Physics. The SAT-TPC was tested with Ar-CO<sub>2</sub> (90:10) and Ar-iC<sub>4</sub>H<sub>10</sub> (95:5) at atmospheric pressure. The Micromegas detector was first characterized in a small test chamber to optimize the ratio between the drift and amplification fields to maximise electron transparency. After establishing the optimal operating parameters, the same Micromegas detector was employed as the readout plane of the SAT-TPC prototype. The energy resolution for <sup>55</sup>Fe and <sup>241</sup>Am was estimated. A straightforward analysis of  $\alpha$ -particle tracks has been carried out, demonstrating the pad plane's capability to accurately reconstruct the direction and length of trajectories. A hydrodynamic model based on Geant4, Garfield++ and COMSOL was used to emulate the reconstructed  $\alpha$  tracks in the active gas volume. The results show good agreement with simulations, confirming the accuracy of the models employed for  $\alpha$ -particles in Ar-CO<sub>2</sub> (90:10) and Ar-iC<sub>4</sub>H<sub>10</sub> (95:5) gas.

**Keywords:** Micromegas, Active-target TPC, Energy resolution,  $\alpha$  tracking, Gas gain

# 1 Introduction

Micromegas (MICRO-MEsh Gaseous Structure) is a type of gaseous detector widely used in experimental particle and nuclear physics due to its excellent spatial resolution, high rate capability, and robustness. Micromegas based Active-Target Time Projection Chamber (AT-TPC) in recent days has emerged as a crucial tool for carrying out nuclear astrophysics research to envisage the stellar nucleosynthesis as the origin of elements and provide essential data for different models and predictions. For example, estimation of photonuclear reaction cross-sections at astrophysical energies, or determination of branching ratio of Hoyle state decay mechanisms are of paramount importance to elucidate the carbon and oxygen synthesis in stellar medium, which have been explored using the AT-TPC in order to achieve high-precision results [1, 2].

AT-TPC is a gas-filled particle detection device which provides near- $4\pi$  coverage and enables efficient three-dimensional tracking that allow precise measurement of nuclear reaction or decay cross-sections through kinematic reconstruction and identification of particles utilizing energy loss information. The unique dual functionality of the gaseous content of the device as both target and active detection medium has offered several advantages to circumvent several issues of the traditional techniques that employ solid targets and solid-state detector arrays, such as energy straggling, background, particle identification ambiguity, pile-up, limited energy resolution, etc., not to mention the convenience of setting up and operating a stand-alone compact device in the experiments. All these factors together have caused a paradigm shift in the experimental technique to explore wide range of research problems in the nuclear and nuclear astrophysics fields spanning over shell evolution, cluster structure, exotic decays, giant resonances, fusion-fission, etc. Several examples of such applications of this novel device include MAYA [3], MUSIC [4], MAIKo [5], ACTAR [6], AT-TPC [7], ELITPC [8], TexAT [9], MATE [10], GADGET [11], etc.

The high-precision three-dimensional tracking capability of AT-TPC has enabled observation of the extremely rare direct decay channel of the Hoyle state in  $^{12}\text{C}$ , leading to precise branching ratio measurements using both direct (0.043%) [2] and indirect (0.00057%) [12] methods, while the best limit from silicon detectors achieved so far is 0.019% [13]. With an aim to explore the Hoyle state decay mechanism and the branching ratio of the direct decay with high precision, the R&D work has been undertaken to develop an AT-TPC device at the laboratory of Saha Institute of Nuclear Physics, namely, Saha AT-TPC (SAT-TPC). To obtain a guideline on optimal design and operation of the SAT-TPC, the performance of the device for the adopted design parameters and operating conditions has been simulated using a hydrodynamic model [14]. In view of the future data-taking campaign, a data analysis protocol has been developed as well for classification of the direct decay using Convolutional Neural Network (CNN) [15]. The present paper reports characterization and optimization of bulk Micromegas detector [16] for its implementation as the end-plate readout in the SAT-TPC device. In this context, detailed experimental studies of gain, energy resolution, and  $\alpha$ -track reconstruction performance of the Micromegas in a small prototype setup, like the SAT-TPC, have been carried out using different gas mixtures. Comparison between experimental measurements and numerical simulations, performed by

using Geant4 [20], Garfield++ [17], and COMSOL [19], has been made to envisage the device dynamics and optimize the relevant design and operational parameters.

The article is organized in the following order. Section 2 describes the Micromegas prototype and its characterization. Section 3 presents the prototype SAT-TPC design, electric-field configuration, and measurement results. Section 4 details the numerical simulation of primary charge transport and track reconstruction. Finally, Section 5 provides the summary and conclusions.

## 2 Characterization of the Micromegas

A bulk Micromegas with amplification gap of  $128 \mu\text{m}$  has been opted for the two-dimensional position readout plane of the SAT-TPC. A prototype of active area  $10 \times 10 \text{ cm}^2$  has been subjected to the characterization studies for optimizing its operational parameters. The top views of the same are presented in figure 1 to show the features. The images have been taken using a calibrated microscope (Olympus MX51) using optical zoom 50X and 10X respectively. The mesh is calendered with stainless steel wires with diameter of about  $18 \mu\text{m}$  and  $63 \mu\text{m}$  pitch. The pillars used to maintain the amplification gap and mechanical rigidity of the mesh have diameter of  $400 \mu\text{m}$  which are fixed with a periodicity of approximately  $2 \text{ mm}$ . The readout plane of the Micromegas has 10 strips with width  $0.95 \text{ cm}$  which are separated by a gap of  $0.05 \text{ cm}$ .

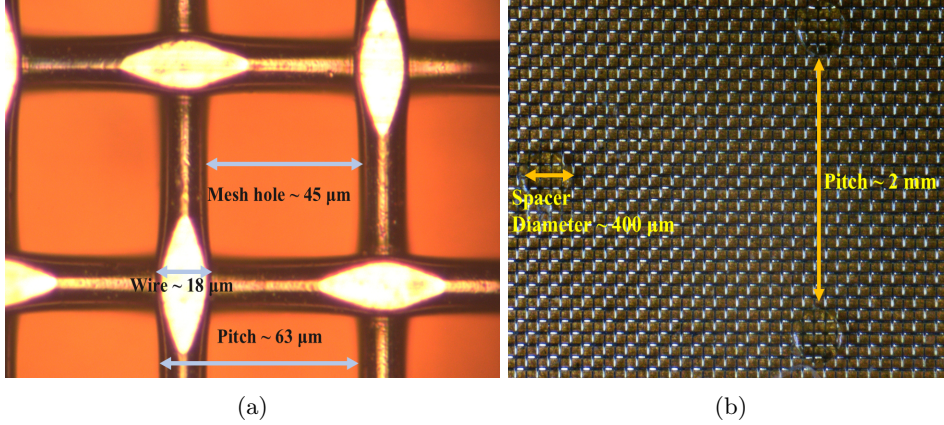


**Fig. 1:** Images of (a) Stainless-steel wire mesh with  $\sim 63 \mu\text{m}$  pitch, (b) Mesh surface showing supporting pillars of  $\sim 400 \mu\text{m}$  diameter and  $2 \text{ mm}$  pitch.

### 2.1 Test setup

The electron transparency is a key characteristic feature to be investigated in order to determine the working regime of the Micromegas. It has been studied using  $^{55}\text{Fe}$  X-ray source in a test setup, as shown schematically in figure 2. The Micromegas detector was housed in a leak-proof stainless steel test chamber with an internal volume

of  $6.5 \times 40 \times 40 \text{ cm}^3$ , as shown in Fig. 2. The chamber was flushed with premixed gases, specifically Ar+CO<sub>2</sub> (90:10) and Ar+iC<sub>4</sub>H<sub>10</sub> (95:5), maintained at atmospheric pressure. The drift electric field was established by applying negative high voltage to the cathode plate using a CAEN power supply, while the micromesh was biased independently to create the amplification field. For signal processing, the anode strips were connected to a low-noise, 8-channel charge-sensitive preamplifier (model: CAEN A1422). The resulting analog signals were fed into a CAEN V1730S digitizer for data recording. The data acquisition was controlled using the Compass software. A <sup>55</sup>Fe X-ray source was mounted above the cathode plate to irradiate the active area for characterization.

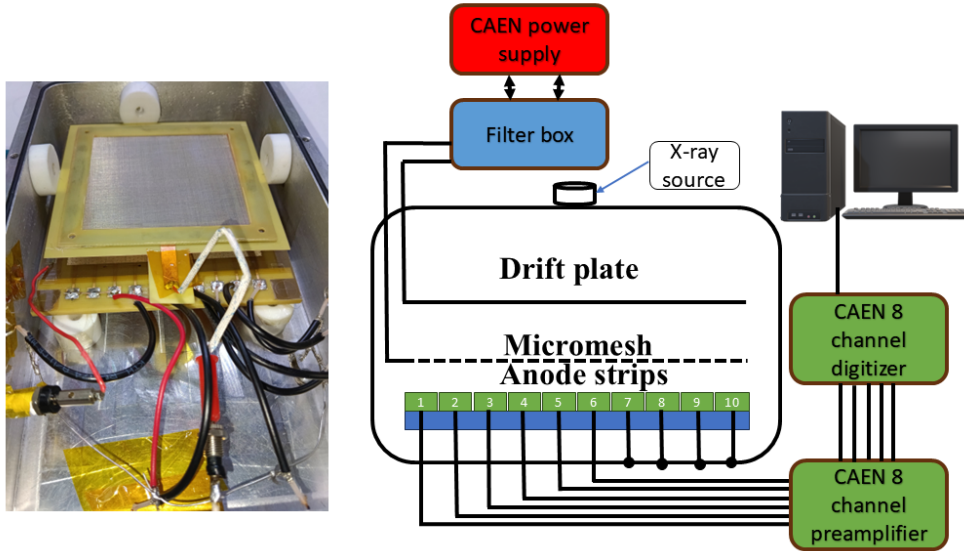
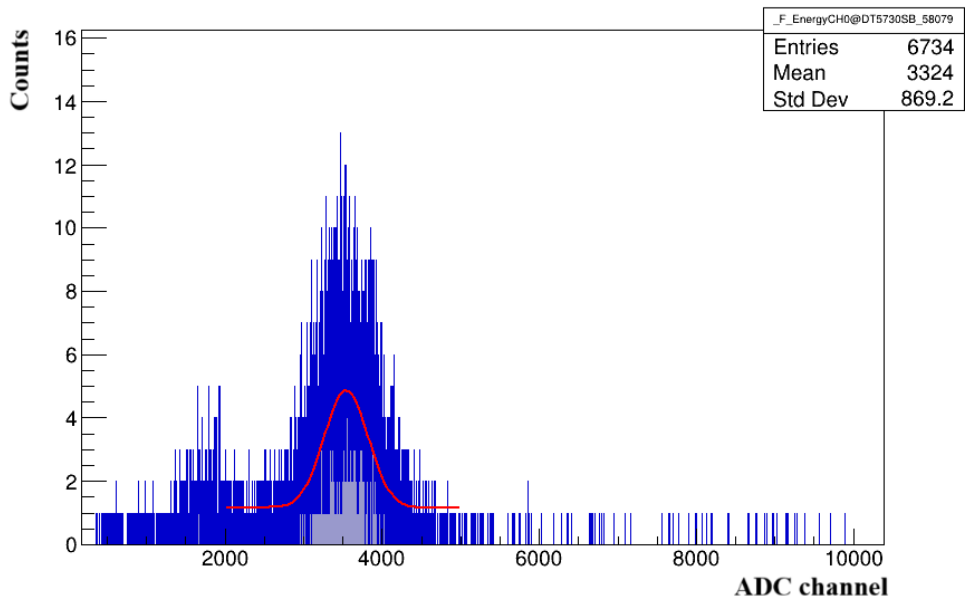


Fig. 2: Experimental setup with Micromegas

## 2.2 Electron transparency

Electron transparency ( $\mathcal{T}$ ) is a fundamental parameter of the Micromegas detector, defined as the ratio of primary electrons from the drift region that successfully pass through the micro-mesh openings into the amplification gap to the total number of electrons reaching the mesh. To optimize this parameter, a systematic exploration of electron transmission was carried out by independently varying the drift field ( $E_{drift}$ ) and amplification field ( $E_{amp}$ ). While the amplification field was held constant at optimized values—40.8 kV/cm for Ar+CO<sub>2</sub> (90:10) and 26.5 kV/cm for Ar+iC<sub>4</sub>H<sub>10</sub> (95:5)—the drift field was scanned across a range of approximately 100 to 1000 V/cm.

A typical spectrum obtained with a 5.9 keV <sup>55</sup>Fe X-ray source, recorded by the anode plane, is depicted in figure 3.



**Fig. 3:** Typical 5.9 keV X-ray spectrum recorded by the anode plane of prototype Micromegas operated with Ar+CO<sub>2</sub> (90:10) mixture at atmospheric pressure

The measured electron transparency of the 128  $\mu\text{m}$  bulk Micromegas operated with the two gas mixtures have been plotted in figure 4 as a function of the drift field where the results are comparable to previous work [21]. Electron transmission has been observed to increase with the drift field up to a plateau region, corresponding to full transparency, beyond which it has decreased at higher fields due to over-focusing effects near the mesh [21]. This plateau defines the optimal operating regime for the Micromegas detector, where both gain and energy resolution remain stable by maximising the electron extraction from the drift region to amplification volume.

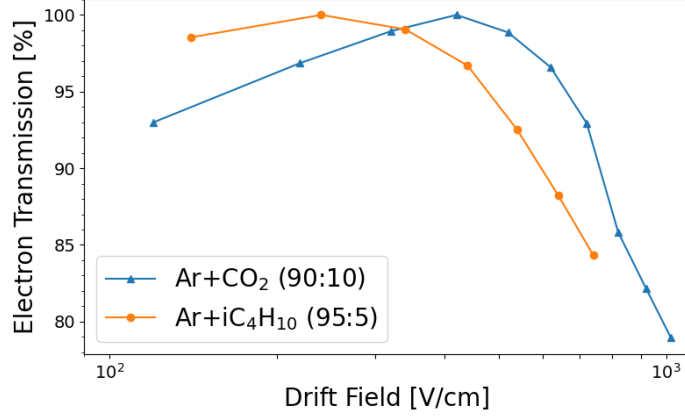


**Fig. 4:** Electron transmission as a function of drift field for the Micromegas detector. The measurement was performed at a constant amplification field of 40.8 kV in Ar+CO<sub>2</sub> (90:10) and 26.5 kV in Ar+iC<sub>4</sub>H<sub>10</sub> (95:5) mixtures at atmospheric pressure

### 3 SAT-TPC prototype

The Micromegas has been subsequently integrated in a prototype SAT-TPC setup with comparatively long drift region. This setup is important for studying the Micromegas performance under realistic conditions, taking into account the effects of the extended drift volume, field-cage geometry, and gas circulation system.

#### 3.1 Setup

A leak-proof chamber with internal volume  $6.5 \times 40 \times 40 \text{ cm}^3$  has been built to circulate the premixed Ar+CO<sub>2</sub> (90:10) and Ar+iC<sub>4</sub>H<sub>10</sub> (95:5) at atmospheric pressure. The cathode plate has been positioned 4 cm above the Micromegas followed by two field-shaping electrodes spaced by 1.34 cm to ensure a uniform electric field in the active region. The cathode and the two field-shaping electrodes have been connected in series using 10M $\Omega$  resistors. The cathode has been biased negatively and the field cage thus has acted as a voltage divider. The setup is schematically represented in figure 5 while the pictures of the prototype SAT-TPC and the Micromegas readout plane are shown in figure 6. Suitable arrangements have been made for mounting the Fe<sup>55</sup> X-ray source and Am<sup>241</sup>  $\alpha$ -source within the chamber for carrying out necessary measurements.

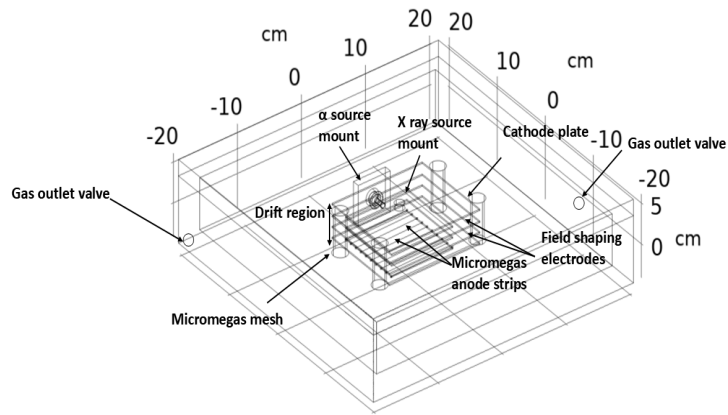


**Fig. 5:** Schematic diagram of the prototype SAT-TPC setup

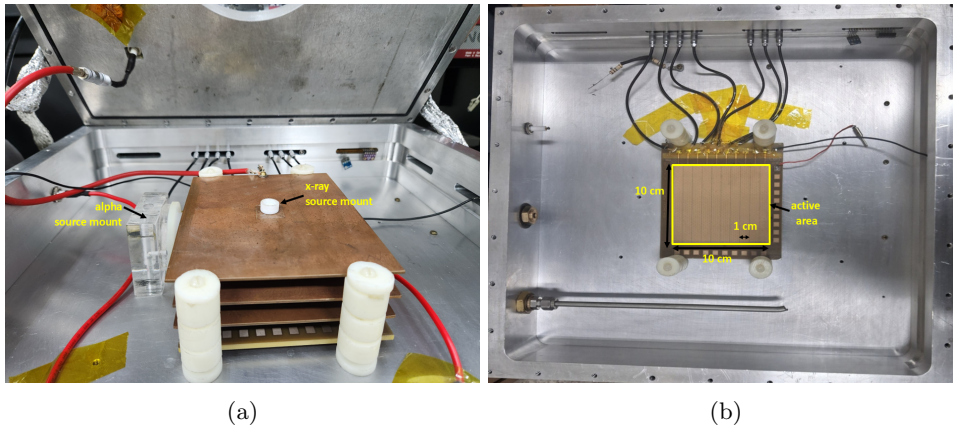


**Fig. 6:** (a) Prototype SAT-TPC setup with X-ray and  $\alpha$ -source mounts, and (b) Micromegas detector active area with 1 cm pitch readout strips.

The anode plane of the Micromegas comprises of 10 readout strips of width 9.5 mm with 0.5 mm gap between adjacent strips. Out of 10, 7 strips were used while the rest 3 were kept grounded due to limited number of readout electronics. Measurements with the  $^{55}\text{Fe}$  X-ray source were performed with signals taken from both the micromesh and the readout strips.

### 3.2 Gas gain

The number of the primary electrons here was estimated from the GARFIELD++ code using the HEED [22] toolkit that implements Photo Absorption Ionization (PAI) model. For each X-ray event, HEED calculates the energy loss and generates ionization clusters along the photon interaction track. Each cluster corresponds to a localized group of electron-ion pairs created in a single ionization act, and the total number of primary electrons is obtained by summing the electrons from all clusters produced in an event. The histograms of primary ionization electrons produced by 5.9 keV X-ray in Ar+CO<sub>2</sub> (90:10) and Ar+iC<sub>4</sub>H<sub>10</sub> (95:5) gas mixtures are shown in figure 7. The resulting distributions exhibit mean values of 211 and 218 primary electrons, respectively. These values are consistent with expectations of HEED toolkit integrated within Garfield++ [22], reflecting the dependence of primary ionization yield on gas composition. To determine the Micromegas gain, both the cathode and mesh voltages were

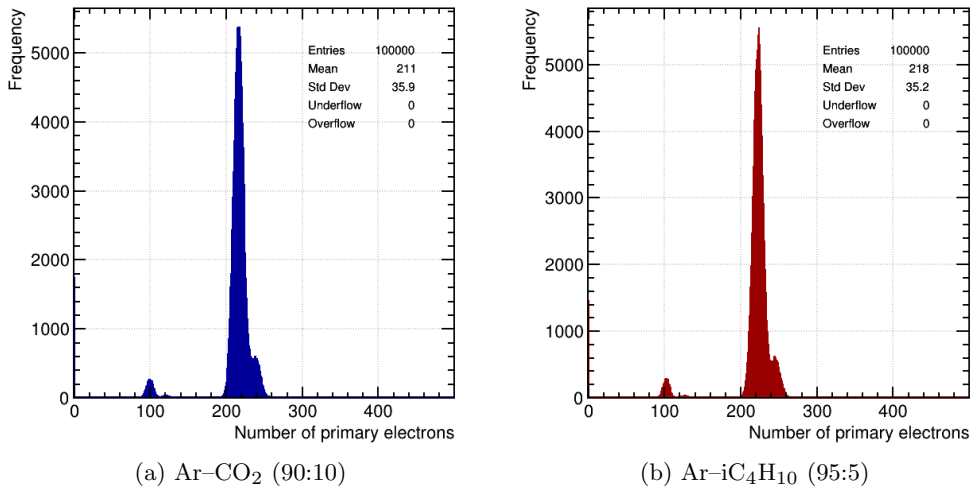


**Fig. 7:** Number of primary electrons produced by 5.9 keV X-rays in different gas mixtures at atmospheric pressure and room temperature, obtained from Garfield++ simulations.

varied systematically while maintaining equal potential differences between successive electrodes and the mesh. The gain was determined as a function of the drift field by varying mesh voltage from  $-225\text{V}$  to  $-385\text{V}$ , and the corresponding cathode voltage from  $-900\text{V}$  to  $-1540\text{V}$ . Charge signals induced on the readout strips were first converted into voltage and then amplified using 8-channel preamplifier (*model: CAEN A1422*). The resulting analog voltages were digitized and recorded with a digitizer (*model: CAEN V1730S*) for offline analysis. All measurements were performed using Ar+CO<sub>2</sub> (90:10) and Ar+iC<sub>4</sub>H<sub>10</sub> (95:5) gas mixtures at atmospheric pressure. A <sup>55</sup>Fe source with an activity of 8 mCi was placed on a mount above the cathode plate for

the gain measurement. During data collection, the detector chamber was maintained at a temperature of  $24 \pm 1^\circ\text{C}$  and a pressure of  $754 \pm 4.5$  Torr.

Since the source was placed near the center of the cathode plate, the fifth and sixth strips typically recorded the largest signals (Fig. 8a). The energy spectrum was obtained from the mesh signal recorded in the digitizer *CAEN V1730S* following preamplification with *A1422* which is shown in figure 8b.

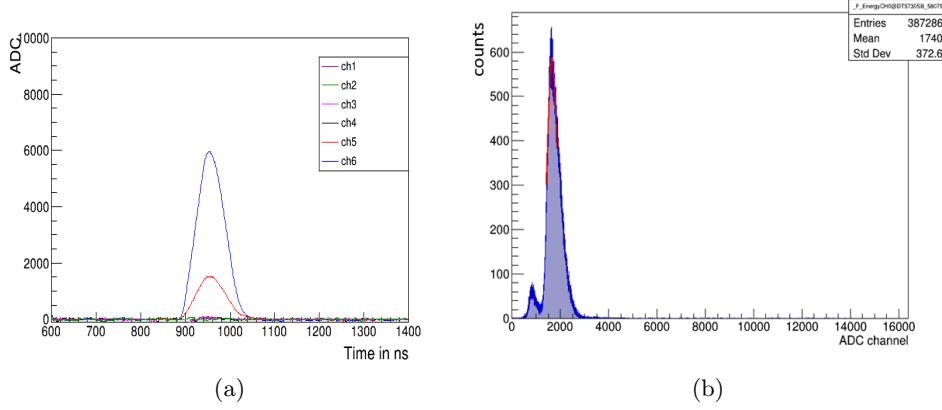


**Fig. 8:** (a) Readout signals, and (b) energy spectrum of the X-ray from  $\text{Fe}^{55}$ -source.

The gas gain  $G$  can be defined as the ratio of collected number of electrons to the primary electrons [21] which can be expressed as follows.

$$G = \frac{Q_{\text{col}}/e}{N_p}, \quad (1)$$

where  $Q_{\text{col}}$  is the collected charge,  $e$  is the electronic charge and  $N_p$  is the number of primary electrons.

To determine the number of collected electrons, the measured charge is used which is obtained from the ADC counts recorded from the readout strips. To convert the ADC counts obtained from the digitizer to collected charge ( $Q_{\text{col}}$ ), an RC-injection calibration was performed through the entire electronic chain of the readout strips. The calibration plot of the charge versus ADC counts is shown in figure 9.

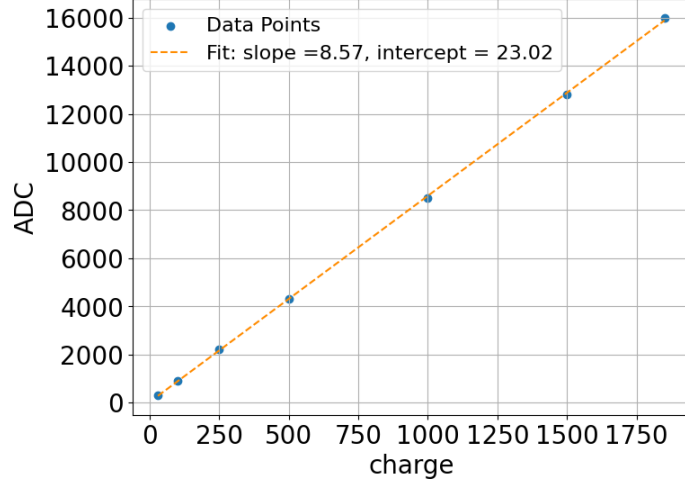


**Fig. 9:** Calibration plot used to convert ADC counts to collected charge.

The calibration fit as shown in figure 9 was used to convert the ADC count to charge (fC) using the following expression.

$$\text{charge [fC]} = \frac{\text{ADC [counts]} - 23.02}{8.57}. \quad (2)$$

Figure 10 presents the gain curves for Ar+CO<sub>2</sub> (90:10) and Ar+iC<sub>4</sub>H<sub>10</sub> (95:5), measured with the <sup>55</sup>Fe-source where the results are comparable to previous work [21]. Both mixtures exhibit the expected exponential dependence of gain on the amplification field. For Ar+CO<sub>2</sub>, noticeable amplification starts at approximately 36 kV/cm, whereas Ar+iC<sub>4</sub>H<sub>10</sub> shows measurable gain at slightly lower fields. The higher gain of Ar+iC<sub>4</sub>H<sub>10</sub> at elevated fields can be attributed to its enhanced Penning effect and lower ionization potential [24].

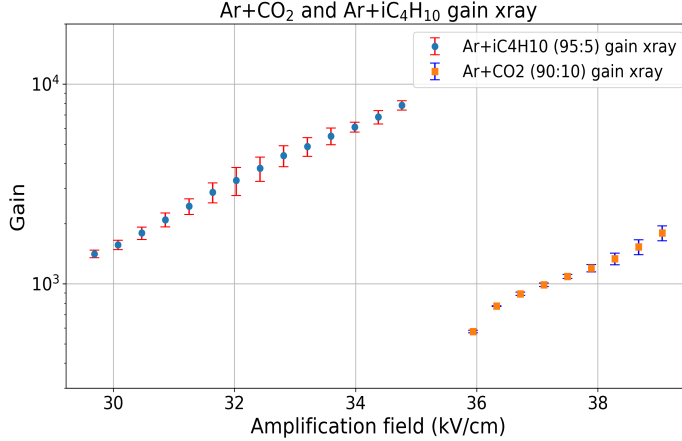


**Fig. 10:** Gain measured in Ar+CO<sub>2</sub> (90:10) and Ar+iC<sub>4</sub>H<sub>10</sub> (95:5) using the <sup>55</sup>Fe X-ray source.

## 4 Simulation of prototype SAT-TPC

A simulation framework based on hydrodynamic approach was developed to study the performance of an active-target TPC including the space-charge effect on it [18]. In this work, the same model was used to estimate the primary charge arriving at the Micromegas before amplification. The model treats the transport of negative and positive charges in the gas using hydrodynamic-like equations implemented in COMSOL Multiphysics [19]. GEANT4 [20] was used to model the initial ionization by particles, while MAGBOLTZ [27] provided transport parameters (drift velocity and diffusion coefficients) for the gas mixtures. The electric field was computed in COMSOL.

### 4.1 Electric field simulation

The electric field distribution in the SAT-TPC prototype setup has been simulated using COMSOL for the given geometry. The result of the simulation is shown in figure 11 where the electric field strength has been represented by the color coding, while the black curves have depicted the field lines, illustrating the direction of the field. It may be observed that in the central drift region, the simulated electric field lines are straight and parallel, confirming a uniform drift field which is an essential condition for accurate three dimensional track reconstruction. In contrast, near the edges and around the field-shaping electrodes, the lines have bent and clustered, indicating localized field distortions. For the applied voltages of  $-1200$  V at the cathode and  $-300$  V at the Micromegas mesh, the electric field in the central active region was approximately  $228$  V/cm. The drift and amplification field ratio of

$$\frac{E_{\text{drift}}}{E_{\text{amp}}} \approx 9.6 \times 10^{-3},$$

used in the prototype SAT-TPC, which closely matches the optimal values obtained from the Micromegas characterization measurements.

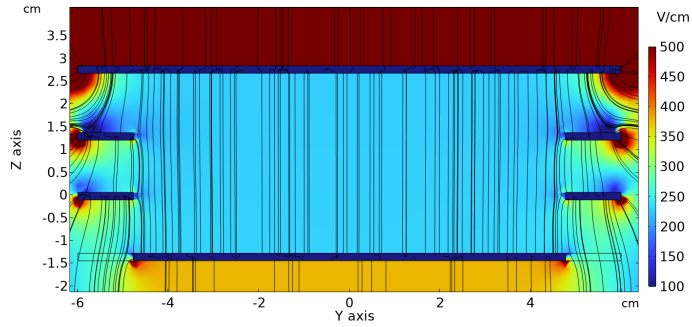


**Fig. 11:** Electric field magnitude (in V/cm) inside a cross-section of the prototype SAT-TPC.

The first-stage ionization by 5.48 MeV  $\alpha$  particles from  $^{241}\text{Am}$  was modeled in GEANT4 using low-energy physics lists (Penelope, Livermore, and PAI). MAGBOLTZ supplied the drift velocity and diffusion parameters for Ar-CO<sub>2</sub> (90:10) and Ar-iC<sub>4</sub>H<sub>10</sub> (95:5). These parameters were used to simulate temporal evolution and spatial spread of primary electron clusters in the drift volume.

One hundred  $\alpha$ -track events were generated in GEANT4 with the source placed 2 cm from the active volume (at  $X = -7$  cm), and the resulting seed-cluster schematic from COMSOL for Ar-CO<sub>2</sub> (90:10) is shown in Fig. 12.

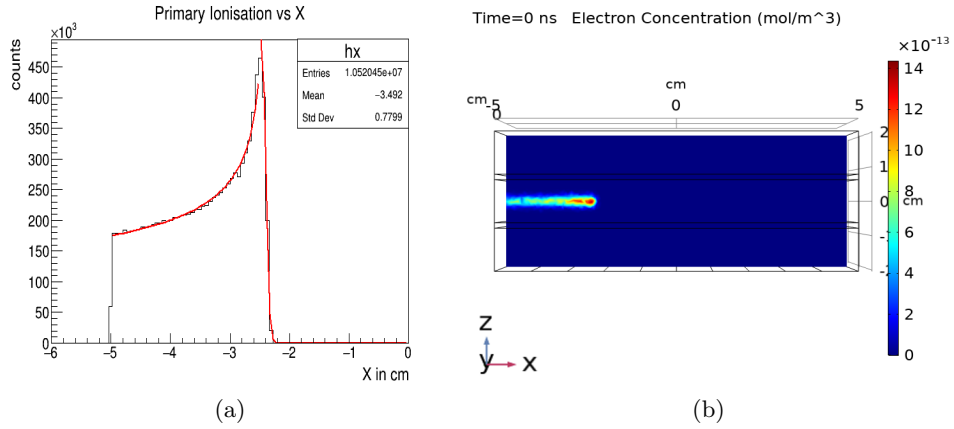


**Fig. 12:** (a)  $\alpha$  event simulated in Geant4. (b) Seed cluster of primary ionization simulated in COMSOL for Ar-CO<sub>2</sub> (90:10).

The drift and diffusion parameters were used to simulate the temporal evolution of primary electron and ion concentrations. The induced currents on the anode readout pads (dimensions  $10\text{ cm} \times 1\text{ cm}$ ) were calculated as the electrons propagated through the drift volume. These current signals were integrated to obtain the equivalent collected charge on the readout strips, as illustrated in Fig. 13.

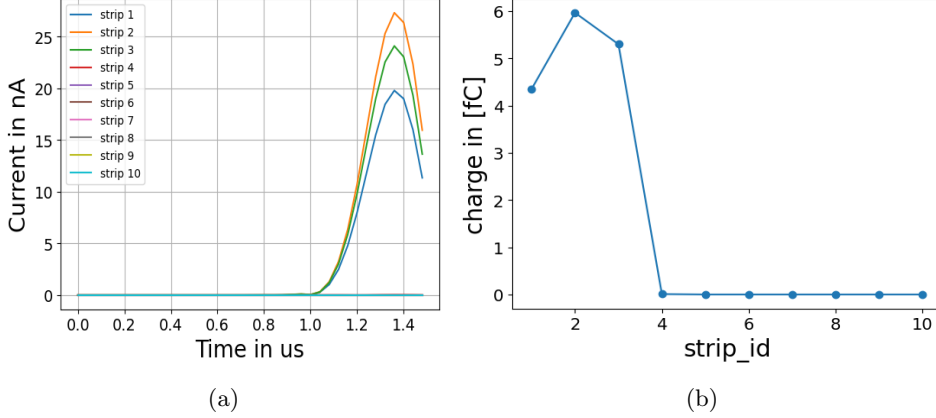


**Fig. 13:** (a) Current generated by an  $\alpha$  track. (b) Primary ionization charge deposited by an  $\alpha$ , as obtained from COMSOL simulations.

## 4.2 Energy resolution

At the operating field where the  $^{55}\text{Fe}$  peak was evaluated, the measured FWHM energy resolutions are 9.3% for Ar+CO<sub>2</sub> (90:10) and 8% for Ar+iC<sub>4</sub>H<sub>10</sub> (95:5). The better resolution observed in the isobutane mixture likely reflects improved statistical charge collection and reduced gain fluctuations, consistent with trends reported in GEM-based studies [25] and Micromegas performance measurements [26]. Error bars are small across the dataset, indicating stable measurement conditions. No gain saturation was observed within the measured range.

## 4.3 $\alpha$ -tracking

For  $\alpha$ -track measurements using the  $^{241}\text{Am}$  source, the mesh signal was used as the trigger. The same electronic chain described earlier was used for these measurements. The Micromegas strips ( $10 \times 10\text{ cm}^2$  active area) were oriented perpendicular to the  $\alpha$  source and placed under the field cage. The  $^{241}\text{Am}$  source was collimated using a nylon tube with a 2 mm diameter and positioned 2 cm above the mesh plane at the center of the Z direction of the field cage to ensure  $\alpha$ -particles were approximately perpendicular to the anode strips. The mesh signal from the preamplifier was used to trigger the strip readout. Signals from strips falling within a 1  $\mu\text{s}$  window around the mesh trigger were recorded using the Compass data-acquisition software. Six electronic

channels were used for the Micromegas readout and one electronic channel from its mesh for trigger in the experiment.

An example of signals from strips 1-6 in Ar+CO<sub>2</sub> (90:10) at atmospheric pressure is shown in figure 14. The strip waveforms display the expected variation in pulse height across adjacent channels due to the transverse diffusion of the drifting electron cloud and the resulting charge sharing among neighboring strips. The corresponding integrated charge distribution provides the lateral charge-deposit profile on the pad plane, which is subsequently used to determine the hit position and reconstruct the projected  $\alpha$ -particle track in the SAT-TPC prototype.

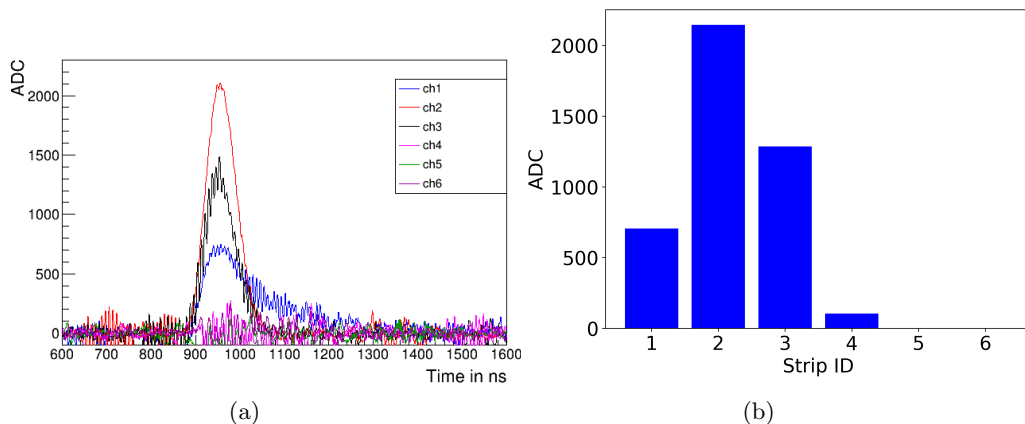


**Fig. 14:** (a) Example strip signals from the six channels connected to the electronic chain. (b) Charge-deposit profile along the strips for an  $\alpha$  event.

#### 4.4 Gas gain for $\alpha$ -source

We determined the gain for  $\alpha$  tracks using the method described in Section 3.2. For 5.48 MeV  $\alpha$  particles in Ar+CO<sub>2</sub> (90:10) and Ar+iC<sub>4</sub>H<sub>10</sub> (95:5) at atmospheric pressure, the Micromegas provides effective gains between  $\sim 10$  and 110 for amplification fields of 17-30 kV/cm, as shown in figure 15. The exponential rise of gain with field and the systematically higher gain in Ar+iC<sub>4</sub>H<sub>10</sub> are consistent with expectations for Penning-enhanced argon-isobutane mixtures [24]. The absolute gain values are comparable to those reported for Micromegas with similar geometries and operating pressures in Ar-based mixtures [28], but remain below the higher gains obtained in configurations employing additional preamplification stages or operated at larger amplification fields [29, 30].

The energy resolution for  $\alpha$  tracks was studied for both argon-based gas mixtures at atmospheric pressure. The micromesh voltage was set to  $-340$  V (yielding gain  $\sim 29$ ) for Ar+CO<sub>2</sub> (90:10) and to  $-240$  V (gain  $\sim 23$ ) for Ar+iC<sub>4</sub>H<sub>10</sub> (95:5). The corresponding cathode voltages were  $-1360$ V and  $-960$ V, respectively. The  $\alpha$  range in both gases is approximately 5 cm; since the source was mounted 2 cm from the active

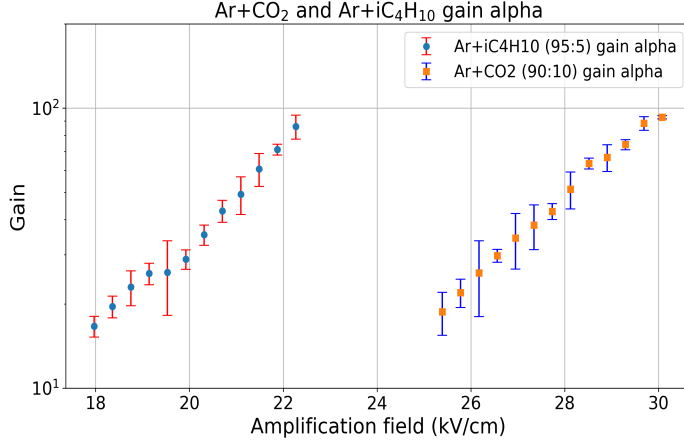


**Fig. 15:** Gain measured in Ar-CO<sub>2</sub> (90:10) and Ar-iC<sub>4</sub>H<sub>10</sub> (95:5) with the  $\alpha$  source.

volume, some energy was deposited in the dead region outside the active volume. The effective energy deposited in the active region of the TPC is about 3.43 MeV. Energy spectra obtained from the sum of strip charges for both gases are shown in figure 16.

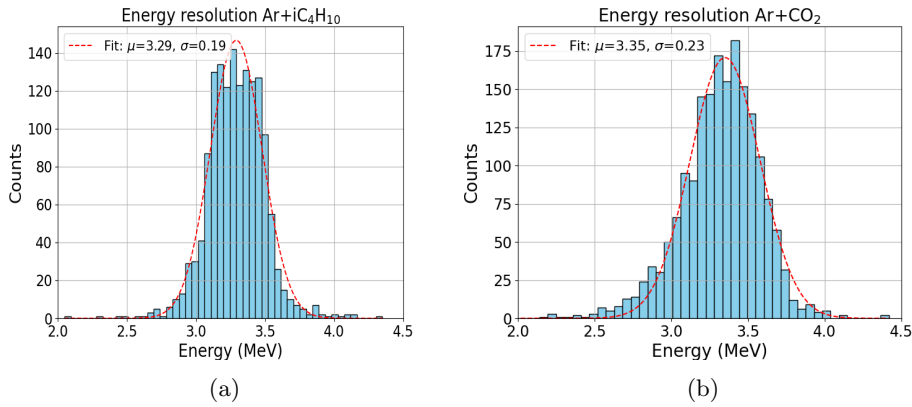


**Fig. 16:** Spectrum of the energy deposited by  $^{241}\text{Am}$   $\alpha$ -particles in (a) Ar-CO<sub>2</sub> (90:10) and (b) Ar-iC<sub>4</sub>H<sub>10</sub> (95:5).

The energy spectra in Fig. 16 display a pronounced peak near 3.35 MeV. The measured energy resolutions are  $\sigma = 6.9\%$  for Ar+CO<sub>2</sub> (90:10) and  $\sigma = 5.7\%$  for Ar+iC<sub>4</sub>H<sub>10</sub> (95:5), corresponding to FWHM values of approximately 16.1% and 13.6%, respectively. The improved resolution in the isobutane mixture is consistent with its reduced electron diffusion and enhanced Penning transfer. The relatively coarse 1 cm strip pitch also contributes to the peak broadening, as the several-centimeter

$\alpha$  tracks span only a few readout strips, increasing charge-collection variance. The present results fall within the range typically observed for bulk Micromegas readouts in AT-TPC- and TexAT-type systems operated at atmospheric pressure [9, 31], and are naturally broader than the  $\sim 2\%$  FWHM achieved in high-pressure microbulk detectors [28]. Overall, the measured resolutions are consistent with expectations for a 128  $\mu\text{m}$ -gap bulk Micromegas with 1 cm segmentation operated at 1 atm. Future work will aim to improve energy resolution by employing finer readout segmentation which enhances position resolution and track fitting through superior spatial sampling as well as operating at lower pressures and exploring hybrid or microbulk Micromegas configurations.

## 5 Summary and conclusion

We have designed and characterized a Micromegas-based prototype SAT-TPC and assessed its performance using X-ray and  $\alpha$  sources.  $\alpha$ -track reconstruction from the pad-plane signals shows good agreement with numerical simulations carried out using GEANT4, Garfield++ and COMSOL, demonstrating that the prototype can reliably recover the projected track length and direction. Using a  $^{55}\text{Fe}$  source, the Micromegas was optimized in Ar-CO<sub>2</sub> (90:10) and Ar-iC<sub>4</sub>H<sub>10</sub> (95:5) at atmospheric pressure, providing stable operation in the full-transparency region and suitable gain for TPC readout. With a  $^{241}\text{Am}$  source, the detector delivered effective gas gains between  $\sim 10$  and 110 for 5.48 MeV  $\alpha$  tracks and energy resolutions of  $\sigma = 6.9\%$  in Ar-CO<sub>2</sub> and  $\sigma = 5.7\%$  in Ar-iC<sub>4</sub>H<sub>10</sub>, consistent with expectations for a 128  $\mu\text{m}$ -gap bulk Micromegas operated at 1 atm. The observed energy resolutions and tracking capability indicate that Micromegas is a promising readout option for future active-target TPCs aimed at low-energy nuclear-reaction studies.

Future work will focus on improving the energy resolution and tracking granularity by employing finer readout segmentation, exploring operation at lower pressure, and performing in-beam tests to validate the SAT-TPC performance under realistic experimental conditions.

**Acknowledgements.** The authors would like to thank Mr. Nilanjan Biswas for his technical help in assembling the Micromegas detectors. We also acknowledge Dr. Abhik Jash, Dr. Tanay Dey, Dr. Vishal Kumar and Dr. Subhendu Das for their valuable suggestions and advice in experimental work and data analysis. We also thank Prof. Tinku Sinha, Prof. Anjali Mukherjee, and Prof. Chinmay Basu for their support. The authors acknowledge the support provided by the Saha Institute of Nuclear Physics.

## References

- [1] M. Gai et al., *An optical readout TPC (O-TPC) for studies in nuclear astrophysics with gamma-ray beams at HI $\gamma$ S* Jour. Instrum. **5** (2010) P12004.
- [2] J. Bishop et al., *Almost medium-free measurement of the Hoyle state direct-decay component with a TPC*, Phys. Rev. C **102** (2020) 041303(R).

- [3] C. E. Demonchy et al., *MAYA: An active-target detector for binary reactions with exotic beams*, Nucl. Instr. Meth. **583** (2007) 341.
- [4] M. Avila et al., *Study of  $(\alpha,p)$  and  $(\alpha,n)$  reactions with a multi-sampling ionization chamber* Nucl. Instrum. Meth. A **859** (2017) 63.
- [5] T. Furuno et al., *Performance test of the MAIKo active target*, Nucl. Instrum. Meth. A **908** (2018) 215.
- [6] B. Mauss et al., *Commissioning of the ACTIVE TARGET and Time Projection Chamber (ACTAR TPC)*, Nucl. Instrum. Meth. A **940** (2019) 498.
- [7] T. Roger et al., *Next-generation experiments with the Active Target Time Projection Chamber (AT-TPC) project*, Nucl. Instrum. Meth. A **954** (2020) 161341.
- [8] M. Gai et al., *Time Projection Chamber (TPC) detectors for nuclear astrophysics studies with gamma beams*, Nucl. Instrum. Meth. A **954** (2020) 161779.
- [9] E. Koshchiy et al., *Texas Active Target (TexAT) detector for experiments with rare isotope*, Nucl. Instrum. Meth. A **957** (2020) 163398.
- [10] Z. C. Zhang et al., *Studying the heavy-ion fusion reactions at stellar energies using Time Projection Chamber*, Nucl. Instrum. Meth. A **1016** (2021) 165740.
- [11] Ruchi Mahajan et al., *Time projection chamber for GADGET II*, Phys. Rev. C **110** (2024) 035807.
- [12] R. Smith et al., *Stringent upper limit on the direct  $3\alpha$  decay of the Hoyle state in  $^{12}\text{C}$* , Phys. Rev. C **101** (2020) 021302(R).
- [13] T. K. Ran et al., *New high precision study on the decay width of the Hoyle state in  $^{12}\text{C}$*  Phys. Lett. B **793** (2019) 130.
- [14] P. K. Das et al., *Numerical modelling of Active Target Time Projection Chamber for low-energy nuclear physics*, Jour. Instrum. **20** (2025) P01008.
- [15] P. K. Das et al., *Classification of Hoyle state decay branches in active target time projection chamber using neural network* Jour. Instrum. **20** (2025) P08036.
- [16] I. Giomataris et al., *Micromegas in a bulk*, Nucl. Instrum. Meth. A **560** (2006) 405.
- [17] R. Veenhof, *Garfield, a drift chamber simulation program* Nucl. Instrum. Meth. A **419** (1998) 726-730.
- [18] P. K. Das et al., *Numerical modelling of active target time projection chamber for low-energy nuclear physics* J. Instrum. **20** (2025) P01008.

- [19] COMSOL Multiphysics, *COMSOL Multiphysics*, <https://www.comsol.co.in/comsol-multiphysics>
- [20] S. Agostinelli et al., *GEANT4—a simulation toolkit*, Nucl. Instrum. Meth. A **506** (2003) 250.
- [21] Purba Bhattacharya, *Experimental and numerical investigation on Micro-pattern gas detectors*, Ph.D. Thesis, University of Calcutta, 2014. <https://hdl.handle.net/10603/171687>
- [22] I. Smirnov, *Modeling of ionization produced by fast charged particles in gases*, Nucl. Instrum. Meth. A **554** (2005) 474–493.
- [23] S. F. Biagi, *Monte Carlo simulation of electron drift and diffusion in counting gases under the influence of electric and magnetic fields*, Nucl. Instrum. Meth. A **421** (1999) 234–240.
- [24] Ö. Şahin, İ. Tapan, E. N. Özmanlı, R. Veenhof, *Penning transfer in argon-based gas mixtures*, JINST **5** (2010) P05002.
- [25] P. Roy, P. Bhattacharya, S. Mukhopadhyay, N. Majumdar, *Charge sharing in single and double GEMs*, JINST **16** (2021) C05001.
- [26] P. Bhattacharya, S. Bhattacharya, N. Majumdar, S. Mukhopadhyay et al., *Performance studies of bulk Micromegas of different design parameters*, JINST **9** (2014) C04037.
- [27] S. F. Biagi, *Monte Carlo simulation of electron drift and diffusion in counting gases under the influence of electric and magnetic fields*, Nucl. Instrum. Meth. A **421** (1999) 234–240.
- [28] T. Dafni et al., *Energy resolution of  $\alpha$ -particles in a microbulk Micromegas detector at high pressure argon and xenon mixtures*, Nucl. Instrum. Meth. A **608** (2009) 259–267.
- [29] M. Cortesi et al., *Recent advances with a hybrid micro-pattern gas detector operated in low-pressure  $H_2$  and He for AT-TPC applications*, EPJ Web Conf. **117** (2016) 01007.
- [30] E. Koshchiy et al., *Texas Active Target (TexAT) detector for experiments with rare isotope beams*, Nucl. Instrum. Meth. A **957** (2020) 163398.
- [31] D. Suzuki et al., *The prototype AT-TPC: performance in pure helium and low-pressure gas mixtures*, Nucl. Instrum. Meth. A **691** (2013) 39–54.